Proceedings of ICFDP 8:
Eighth International Congress of Fluid Dynamics & Propulsion
December 14-17, 2006, Sharm El-Shiekh, Sinai, Egypt
ICFDP8-EG-150

SUBSONIC TRIPLE DECK FLOW PAST AN ERODING HUMP

TAREK M. A. EL-MISTIKAWY[a] AND FAYZA M. N. EL-FAYEZ[b]

ABSTRACT

In this paper, the problem of subsonic viscous flow above a horizontal flat plate, having a contamination spot in the form of a hump that erodes shedding its particles to the flow, is treated within the framework of the triple deck theory. The lower deck problem has several new features. It is intrinsically unsteady; i.e. the unsteadiness is due to the flow and not externally imposed on it. It has a moving boundary, as a result of the erosion of the hump both vertically and horizontally. It contains an additional variable, the concentration, together with its transport equation and abruptly changing surface conditions. It involves pressure variation across the lower deck, due to buoyancy. Numerical solutions are obtained starting from a steady hump flow till the complete removal of the hump and its particles from the computational domain. Typical results are presented, showing how the erosion of the hump progresses, and how the contaminant spreads. The roles of diffusivity and buoyancy are also assessed.

KEYWORDS: subsonic triple deck; unsteady hump flow; moving boundary; numerical solution; erosion; contamination; buoyancy

[a] Department of Engineering Mathematics and Physics, Faculty of Engineering, Cairo University, Giza 12211, Egypt.
[b] Department of Mathematics, Girls College of Education, P. O. Box 27104, Riyadh 11417, Saudi Arabia.

1. INTRODUCTION

Flows with mass transfer from a contamination spot are encountered in many situations. Two examples of environmental impact are the contamination of water currents as they run over piles of chemical waste, and of air as wind passes over sand hills.

The presence of the contamination spot triggers viscous/inviscid interaction that can be described only by the triple deck theory [1], which establishes a matched asymptotic structure that explains how a boundary layer flow senses a downstream disturbance and interacts with the outer inviscid flow to facilitate non-singular development past the disturbance. Although the theory is valid as the Reynolds number Re grows indefinitely, it has proven successful at moderate to low values of Re [2].

Numerous steady triple deck problems can be found in the literature. The one of concern to the present work is the flow past a hump. The two dimensional problem was first formulated by Smith [3] and solved numerically by Napolitano et al. [4]. Smith et al. [5] handled a three dimensional hump. Sykes [6] included upper deck stratification in his steady hump flow. The unsteady hump problem was analyzed by Duck [7,8] and Bodonyi et al. [9]. The unsteadiness is externally imposed on the flow, and interest is mainly directed toward wave formation.

The present problem is characterized by several new features that make its numerical solution a difficult task. It is unsteady, the unsteadiness being intrinsic due to the erosion process. The surface of the hump is a moving boundary that diminishes both horizontally and vertically. The concentration enters as an additional variable,

accompanied by its transport equation and surface conditions, which exhibit abrupt changes. Buoyancy results in lateral pressure variations, for which the viscid/inviscid interaction law acts as a far-field boundary condition.

Nonetheless, it was possible to compute a solution, starting from a steady state hump flow till the complete removal of the hump and its contamination particles from the computational domain. The moving boundary of the hump was transformed into a fixed one through an unsteady version of Prandtl's transposition (shift) theorem [10]. The starting steady problem was solved by Veldman's steady solver [11], which was made more efficient by adopting the non-iterative, second order accurate, streamwise marching technique of El-Mistikawy [12]. The solution of the unsteady problem advanced in time in an iterative implicit manner with first order accuracy. All terms in the problem were represented in the new time level; except for the time derivative terms, which used backward representation. The resulting problem, being as close as could be to the steady problem, was solved by the steady solver.

The counterpart of the present problem, when the main flow is supersonic and the buoyancy is neglected, was treated by the authors [13], in a similar fashion. However, the unsteady solver used was based on El-Mistikawy's steady solver of the supersonic lower deck problem [12].

The numerical results, obtained in the present problem, give plausible account of the erosion and contamination processes.

The effect of the diffusion parameter λ, which represents the ratio of concentration to momentum diffusivities, is explored, along with the effect of the buoyancy

parameter α. A decrease in λ is found to cause a decrease in the erosion rate and lateral spread of the contaminant. This is in accordance with the limiting behavior as λ diminishes, which is revealed in [13]. The effect of α is manifested primarily in the lateral variation of the pressure; causing larger surface pressures for larger values of α.

2. STATEMENT OF THE PROBLEM

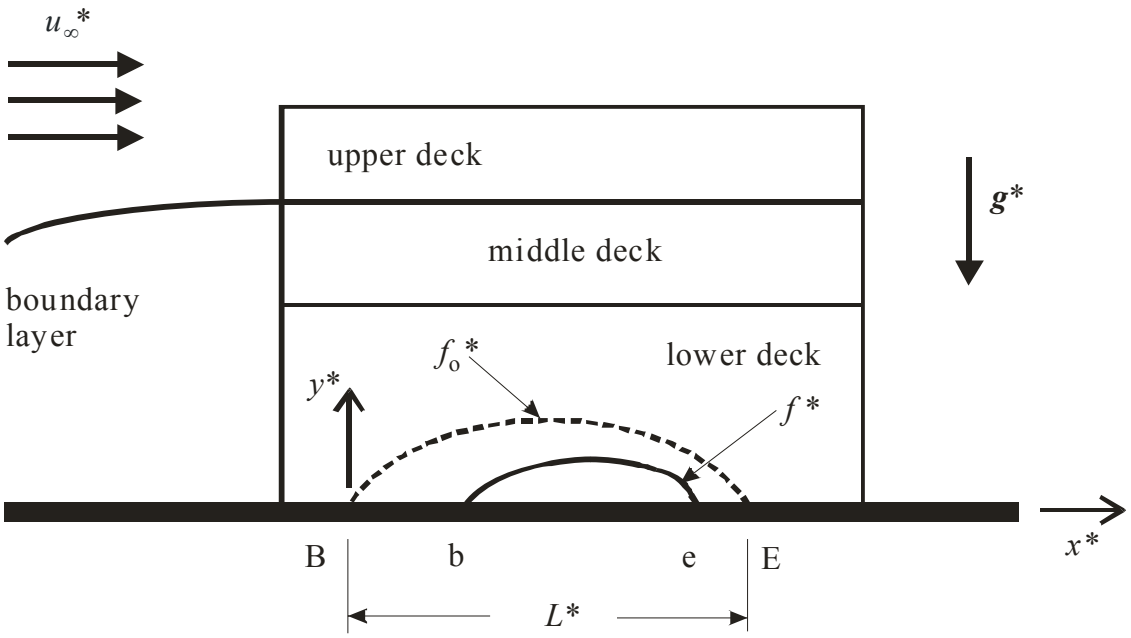

Fig. 1. Flow Configuration

A fully developed two-dimensional laminar compressible boundary layer flow over a horizontal flat plate encounters a contamination spot in the form of a hump (Fig. 1). For time $t^*<0$, the flow is steady with the hump extending a distance L^* from its leading edge B to its trailing edge E. At B, Cartesian coordinate axes: x^* along the plate pointing downstream and y^* vertically upwards opposite to the acceleration of

gravity $\boldsymbol{g}^*$, are introduced. The hump has density σ^* and height described by $y^*=f_o^*(x^*)$ for $0\le x^*\le L^*$. The whole surface is maintained at a fixed temperature θ_s^* at which the clean fluid has density ρ_s^*, and viscosity μ_s^*, and admits saturation concentration c_s, and diffusion coefficient λ_s^*.

Far from the surface, the uncontaminated freestream has uniform velocity u_∞^* in the x^* direction, temperature θ_∞^*, density ρ_∞^*, pressure p_∞^*, sonic speed a_∞^*, and viscosity μ_∞^*. The freestream is subsonic with Mach number $Ma=u_\infty^*/a_\infty^*<1$. The Reynolds number $Re=\rho_\infty^* u_\infty^* L^*/\mu_\infty^*$ is large and relates to a diminishing parameter $\varepsilon=Re^{-1/5}$.

For $f_o^*=O(\varepsilon^2 L^*)$, the boundary layer structure approaching the hump develops into a triple deck structure containing the hump within its lower deck.

At time $t^*=0$, erosion starts as particles of the hump diffuse into the flow to be washed downstream by the oncoming clean fluid. The contamination, therefore, is confined to the lower deck and its downstream continuation. The steady triple deck structure remains intact; however, the lower deck has to be corrected for the unsteady contamination process. The lower deck variables show dependence on the time t^*, which has to be $O(\varepsilon^{-1}L^*/u_\infty^*)$ for the unsteadiness to be of leading order effect. In particular, the hump is described, now, by $y^*=f^*(x^*,t^*)$ for $x_b^*(t^*)\le x^*\le x_e^*(t^*)$, where $f^*(x^*,0)=f_o^*(x^*)$, $x_b^*(0)=x_B^*=0$, and $x_e^*(0)=x_E^*=L^*$. (Henceforth, f^* is extended to describe the entire surface, given zero value outside the interval $x_b^*<x^*<x_e^*$.)

To describe the erosion/contamination process, a version of the triple-deck theory [6] that is applicable to problems whose characteristic length is the streamwise extent

of the source of disturbance, is used. This relates the spread of the contaminant and the rate of erosion directly to the size of the contamination spot, as measured by its length L^*.

The triple deck analysis leads to the following normalized lower deck problem, where a comma followed by a subscript denotes differentiation.

$$U_{,X}+V_{,Y}=0 \tag{1.1}$$

$$U_{,T}+U\,U_{,X}+U_{,Y}\,V+P_{,X}=U_{,YY} \tag{1.2}$$

$$P_{,Y}+\alpha\,C=0 \tag{1.3}$$

$$C_{,T}+U\,C_{,X}+C_{,Y}\,V=\lambda_s\,C_{,YY} \tag{1.4}$$

$$U=0,\ V=F_{,T}=\lambda_s\,C_{,Y},\ C=C_s \qquad \text{at } Y=F(X,T),\ X\in[X_b(T),\,X_e(T)] \tag{1.5a-d}$$

$$U=0,\ V=0=C_{,Y} \qquad \text{at } Y=0,\ X\notin[X_b(T),\,X_e(T)] \tag{1.6a-c}$$

$$U_{,Y}\sim 1,\ U\sim Y-A(X,T),\ C\sim 0 \qquad \text{as } Y\sim\infty \tag{1.7a-c}$$

$$U\sim Y,\ A\sim 0,\ C\sim 0 \qquad \text{as } X\sim-\infty \tag{1.8a-c}$$

$$A\sim 0 \qquad \text{as } X\sim\infty \tag{1.9}$$

$$\pi P\sim -\!\!\!\!\!\!\int_{-\infty}^{\infty}(\xi-X)^{-1}\,A(\xi,T)_{,\xi}\,d\xi \qquad \text{as } Y\sim\infty \tag{1.10}$$

The normalized variables: Cartesian coordinates (X,Y), hump height F, velocity components (U,V), concentration C, pressure P, and time T are related to the corresponding physical variables x^*, y^*, f^*, u^*, v^*, c, p^*, and t^* as follows:

$$x^*=\rho_s^{-1/2}\mu_s^{-1/4}\beta^{-3/4}\tau^{-5/4}\,X\,L^*\ ,\ (y^*,f^*)=\varepsilon^2\,\rho_s^{-1/2}\mu_s^{1/4}\beta^{-1/4}\tau^{-3/4}\,(Y,F)\,L^* \tag{2a,b}$$

$$u^*=\varepsilon\,\rho_s^{-1/2}\mu_s^{1/4}\beta^{-1/4}\tau^{-1/4}\,U\,u_\infty^*\ ,\ v^*=\varepsilon^3\,\rho_s^{-1/2}\mu_s^{3/4}\beta^{1/4}\tau^{-3/4}\,V\,u_\infty^*\ ,\ c=C\,\sigma^*/\rho_s^* \tag{2c-e}$$

$$p^*-p_\infty^*=\varepsilon^2\,\mu_s^{1/2}\beta^{-1/2}\tau^{-1/2}\,P\,\rho^*\,u_\infty^{*2}\ ,\ t^*=\varepsilon^{-1}\,\mu_s^{-1/2}\beta^{-1/2}\tau^{-3/2}\,T\,L^*/u_\infty^* \tag{2f,g}$$

where $\rho_s=\rho_s^*/\rho_\infty^*$, $\mu_s=\mu_s^*/\mu_\infty^*$, $\beta=|1-Ma^2|^{1/2}$ is the Mach factor, while τ represents the

surface shear of the clean boundary layer, as it approaches the hump region. Setting $\beta=\rho_s=\mu_s=1$, and $\tau=0.332$, leads to the case of an incompressible flow.

The lower deck problem (1) has the following new features:

1) It contains the concentration C together with its transport equation (1.4), Stefan condition (1.5c) and saturation condition (1.5d) at the hump surface, no-mass-transfer condition (1.6c) on the flat surface, and clean flow conditions (1.7c) and (1.8c) toward the middle deck and the oncoming boundary layer, respectively.
2) It involves a body force due to gravity that is represented in linear form [14] by the buoyancy term αC in the normal momentum equation (1.3), where the buoyancy parameter α is related to an expansion coefficient associated with diffusion.
3) There is pressure variation across the lower deck, as indicated by equation (1.3).
4) The interaction law (1.10), relating the displacement function A to the pressure P, acts as a boundary condition. Note that ⨍ denotes Cauchy's principal value of the integral.

Problem (1) involves two parameters: the diffusion parameter $\lambda_s=\lambda_s^*/\mu_s^*$ and the buoyancy parameter α, both assumed to be O(1) as $\varepsilon \sim 0$.

The initial conditions at $T=0$ for the unsteady problem (1) result as the solution of the steady problem; which can be obtained by dropping the saturation condition (1.5d) together with all time derivative terms, and setting $F(X,0)=F_o(X)$, $X_b(0)=X_B=0$ and $X_e(0)=X_E$. The concentration equation (1.4) and its boundary conditions (1.6c), (17.c), and (1.8c), then, have the solution of everywhere clean initial flow $C=0$.

3. NUMERICAL SOLUTION

The lower deck problem (1) has the hump as a moving boundary that diminishes in size both laterally and longitudinally, causing intrinsic unsteadiness. The hump height $F(X,T)$ as well as its interval of extent $X_b(T) \le X \le X_e(T)$ has to be determined as a part of the solution.

To handle the moving boundary problem, the hump surface is transferred to the fixed line $y=0$, by applying the unsteady shift

$$y=Y-F \ , \ v=V-U F_{,X}-F_{,T} \qquad (3.1a,b)$$

This is an extension of Prandtl's steady shift [10]

$$y=Y-F_o \ , \ v=V-U F_{o,X} \qquad (3.2a,b)$$

which is applied to the steady problem valid at $T=0$. These shifts result in a discontinuity in v at $T=0$, since the initial value of v (at $T=0$) in the unsteady problem and v in the steady problem differ by $F_{,T}(X,0)$. They also result in discontinuities in v (and consequently in $U_{,X}$) across the lines $X=X_b$ and $X=X_e$ due to the discontinuities in $F_{,X}$.

So shifted, Problem (1) can be rearranged and cast in the following new form

$$Q = P_{,X} \qquad (4.1)$$

$$U_{,X}+v_{,y} = 0, \ \alpha C_{,X}+Q_{,y} = 0 \qquad (4.2a,b)$$

$$U_{,y} = W, \ U_{,T}+U U_{,X}+U_{,y} v+Q+\alpha C F_{,X} = W_{,y} \qquad (4.3a,b)$$

$$C_{,y} = G, \ C_{,T}+U C_{,X}+C_{,y} v = \lambda_s G_{,y} \qquad (4.4a,b)$$

$$U = 0, \ v = 0 \qquad \text{at } y = 0 \qquad (4.5a,b)$$

$$C = C_s \quad \text{for } X \in [X_b, X_e], \ G = 0 \quad \text{for } X \notin [X_b, X_e] \quad \text{at } y = 0 \qquad (4.6a,b)$$

$W \sim 1,\ U \sim y - A + F,\ C \sim 0,\ \pi P \sim -\!\!\!\!\!\!\int_{-\infty}^{\infty} (\xi - X)^{-1} A(\xi,T),_{\xi}\, d\xi$ as $y \sim \infty$ (4.7a-d)

$U \sim y,\ A \sim 0,\ C \sim 0$ as $X \sim -\infty$ (4.8a-c)

$A \sim 0$ as $X \sim \infty$ (4.9)

$\lambda_s G = F,_T$ for $X \in [X_b, X_e]$ at $y = 0$ (4.10)

where the pressure gradient function $Q(X,y,T)$, the shear function $W(X,y,T)$, and the concentration gradient function $G(X,y,T)$ are defined by Eqs. (4.1), (4.3a), and (4.4a), respectively. Eq. (4.2b), which has the same form as the continuity equation (4.2a), is the X -derivative of the normal momentum equation (1.3).

3.1. Time Discretization

To advance from time level n to time level n+1, the time derivatives are expressed with first order accuracy using the backward difference representation $Z,_T = (Z_{n+1} - Z_n)/\omega_n$, where Z stands for U, C, and F with $\omega_n = T_{n+1} - T_n$. All other terms are expressed in the new time level n+1. The resulting problem is as close as possible to the steady problem and is solved, therefore, by a steady solver. All that is needed from the old time level n is U_n, C_n, and F_n. This reduces the storage requirements and avoids having to use v_n, which is discontinuous at the initial time level n=0.

3.2. Iterative Procedure

The steady solver put to use is Veldman's quasi-simultaneous method [11]. It is an efficient iterative procedure that takes, in the k^{th} iteration, an old distribution A^k of the displacement function and produces a new one A^{k+1}.

All equations and conditions in Problem (4) are expressed in the new iteration level k+1, except for Condition (4.7b) which is written as follows

$$U^{k+1} \sim y - A^{k+1} + F^{k} \qquad \text{as } y \sim \infty \qquad (4.7b')$$

That F is given its old value F^{k} is in accord with F being fixed; i.e. known, in the steady problem. (For convenience, the subscript n+1 and the superscript k+1 are dropped, henceforth.)

3.3. Space Discretization

The computational domain covers the region of the Xy-plane described by $X_{-\infty} \le X \le X_{+\infty}$, $0 \le y \le y_{+\infty}$, where $-X_{-\infty}$, $X_{+\infty}$ and $y_{+\infty}$ are large enough to allow for adequate enforcement of the asymptotic conditions (4.7)-(4.9). It is divided into rectangular cells by a grid of (i)-lines $X=X(\mathrm{i})$ and (j)-lines $y=y(\mathrm{j})$. The counter $\mathrm{i}=1\rightarrow\mathrm{I}$ is such that $X(1)=X_{-\infty}$, $X(\mathrm{i_B})=X_{\mathrm{B}}$, $X(\mathrm{i_b})=X_{\mathrm{b}}$, $X(\mathrm{i_e})=X_{\mathrm{e}}$, $X(\mathrm{i_E})=X_{\mathrm{E}}$, and $X(\mathrm{I})=X_{+\infty}$; while the counter $\mathrm{j}=1\rightarrow\mathrm{J}$ is such that $y(1)=0$ and $y(\mathrm{J})=y_{+\infty}$. The typical ij-cell has X-step $\Delta(\mathrm{i})=X(\mathrm{i})-X(\mathrm{i\text{-}1})$ and y-step $\delta(\mathrm{j})=y(\mathrm{j})-y(\mathrm{j\text{-}1})$, and through its midpoint pass the (i-½) and (j-½)-lines.

Veldman's method involves implicit marching in the X-direction that advances the solution iteratively from an i-line to the next, and uses three-point backward representation in the X-direction to achieve second order accuracy. The same level of accuracy is achieved non-iteratively by applying El-Mistikawy's marching technique [12], which employs the following discretization layout: U, C, and P are assigned to the grid points (i,j); v, W, and Q are assigned to the points (i-½,j); A is assigned to the i-lines; and F is assigned to both the i and (i-½)-lines. Eq. (4.1) is centered at the (i-½,j)-points, whereas Eqs. (4.2)-(4.4) are centered at the midpoint of the ij-cell. Central difference expressions, in terms of the abovementioned layout, are used throughout. However, U the coefficient of $U_{,X}$ and $C_{,X}$ in Eqs. (4.3b) and (4.4b)

and $U_{,y}$ in Eqs. (4.3a) and (4.3b) are expressed in terms of U(i-½,j) and U(i-½,j-1), then each U(i-½,j) is expressed backwards as U(i-1,j)+½Δ(i)$U_{,X}$(i-½,j) in Eqs. (4.3b) and (4.4b) and forwards as U(i,j)–½Δ(i)$U_{,X}$(i-½,j) in Eq. (4.3a). For these representations to be second order accurate in the X-direction, $U_{,X}$(i-½,j) may be represented with first order accuracy. At i=2, $U_{,X}$(i-½,j) is set equal to zero, in accordance with Condition (4.8a). Next to the two lines i=i_b and i=i_e where $U_{,X}$ is discontinuous, the respective k^{th} iterate $U^k{}_{,X}$(i+3/2,j) with the representation [U^k(i+2,j)–U^k(i+1,j)]/Δ(i+2) is used to approximate $U_{,X}$(i+½,j) and to represent $U_{,X}$(i+3/2,j). Otherwise, since continuity permits, $U_{,X}$(i-½,j) is approximated by its counterpart at the (i-3/2)-line with the representation [U(i-1,j)–U(i-2,j)]/Δ(i-1). A treatment similar to that of $U_{,y}$ in Eqs. (4.3) is applied to $C_{,y}$ in the corresponding Eqs. (4.4).

At each i-line, the 7J–6 finite difference equations are supplemented, in view of Conditions (4.5)-(4.7), with U(i,1)=0, v(i-½,1)=0, C(i,1)=C_s when i_b<i≤i_e, G(i-½,1)=0 when i≤i_b or i>i_e, W(i-½,J)=1, U(i,J)=y(J)–A(i)+F^k(i), C(i,J)=0, and the interaction law as expressed by Veldman [12]

$$\pi P(i,J)=\beta_{ii}A(i)+\Sigma\beta_{ii'}A(i'<i)+\Sigma\beta_{ii'}A^k(i'>i) \tag{5a}$$

where Σ expresses summation over the indicated values of i′, and

$$\beta_{ii'}=[X(i')-½\Delta(i')-X(i)]^{-1}-[X(i'+1)-½\Delta(i'+1)-X(i)]^{-1} \tag{5b}$$

The resulting equations are solved to yield the 7J unknowns: U(i,j), C(i,j), v(i-½,j), P(i,j), W(i-½,j), G(i-½,j), and Q(i-½,j) for j=1→J; as well as A(i), which is updated to A(i)+r[A(i)–A^k(i)], r being a relaxation factor.

Marching in the X-direction starts at i=2 (where Conditions (4.8) supply the needed values at i=1) and ends when i=I. Next, for $i_b<i\le i_e$, Condition (4.10) is used to determine $F(i-½)$ from $F(i-½)=F_n(i-½)+\lambda\ G(i-½)\omega_n$. The resulting i_e-i_b-1 values together with the end conditions $F(i_b)=F(i_e)=0$ suffice to determine $F(i)$ for $i_b<i<i_e$, when F is represented by quadratic splines so that F and $F_{,X}$ are continuous at each i-line.

Of the k^{th} iterates only $F^k(i)$, $A^k(i)$, $U^k{}_{,X}(i_b+3/2,j)$, $U^k{}_{,X}(i_e+3/2,j)$, $C^k{}_{,X}(i_b+3/2,j)$, and $C^k{}_{,X}(i_e+3/2,j)$ need to be stored for use in the next iteration. Their first iterates (when k=1) are taken from the solution at time level n. The iterative process continues until A and F reach convergence as judged by the satisfaction, everywhere, of the inequalities $\left|A^{k+1}(i)-A^k(i)\right|<\eta_A$ and $\left|F^{k+1}(i)-F^k(i)\right|<\eta_F$ where η_A and η_F are prescribed tolerances. This marks the end of the present time step. The step-by-step advance in time continues until the instant when either $F(i_b+1)$ or $F(i_e-1)$ is less than a prescribed tolerance η_{be}. Then, respectively, i_b is increased by 1 or i_e is decreased by 1; and $F=0$ is enforced there.

The steady problem is obtained by dropping the saturation condition (4.6a) and all time derivatives, and setting $F^k=F_o$, $X_b=X_B$, and $X_e=X_E$; to describe the hump in its initial state. Its solution procedure is equivalent to one time step of the unsteady solver in which P, Q, C, and G are treated as "mechul" functions [15]. The convergence of A starting from its guessed distribution $A=F_o$ marks the end of the solution.

4. IMPLEMENTATION

The numerical method explained above is applied to a hump described by

$F_o=4X(1-X)$; thus having $X_E=1$. The computational domain extended to $X_{-\infty}$= -10, $X_{+\infty}=16$, and $y_{+\infty}=12$. The grid was such that I=131, J=39, $i_B=36$, and $i_E=61$. Variable step sizes in both directions were utilized to suit regions of fast or slow changes. Initially, the X-step size Δ took the values: 0.4 (for $1<i\leq6$ and $116<i\leq131$), 0.3 (for $6<i\leq26$ and $96<i\leq116$), 0.2 (for $26<i\leq36$ and $86<i\leq96$), 0.04 (for $36<i\leq61$and $72<i\leq76$), 0.05 (for $76<i\leq80$), and 0.1 (for $80<i\leq86$). This left a gap of size 0.04 that followed $i=i_E$. It was divided by 10 i-lines into much smaller 11 steps; 5 of size 0.002, 3 of size 0.004, then 3 of size 0.006. As time passed, the end of the hump retracted, by steps of size 0.04, from $i=i_E$ to $i=i_e$. After each retraction, those 11 steps were transferred so that they always followed the new i_e-line. To put this transfer into effect, a linear interpolation is all that is needed in order to produce A(i) at the 10 i-lines $i_e<i<i_e+11$ in their new location. The y-step size δ took the values: 0.02, 0.04, 0.06, and 0.08 each for one step, 0.1 for 2 steps, 0.2 for 6 steps, 0.3 for 8 steps, 0.4 for 10 steps, then 0.5 for the last 8 steps. For convergence tolerances, $\eta_A=\eta_F=\eta_{be}=10^{-4}$ is used. A time step ω of size 0.2 was consistently used, unless a change in i_b or i_e had been anticipated. Then, the instant of change was captured in one or two steps within a time interval of 0.4 involving three steps; each not exceeding 0.2. The suitable value for the relaxation factor r was 0.6 for the steady problem and 0.2 for the unsteady problem. These choices made it possible to proceed with the solution till a hump characterized by saturation concentration $C_s=0.01$ was totally erased, and the contaminant was completely washed out of the computational domain.

To study the effect of the diffusion and buoyancy parameters the values λ=0.5, 1, 2 and 5 with α=0; and α=-10, 0, 10, and 20 with λ=1; were used. The negative value of α corresponds to the case of a light contaminant diffusing into a heavier fluid [14].

5. TYPICAL RESULTS

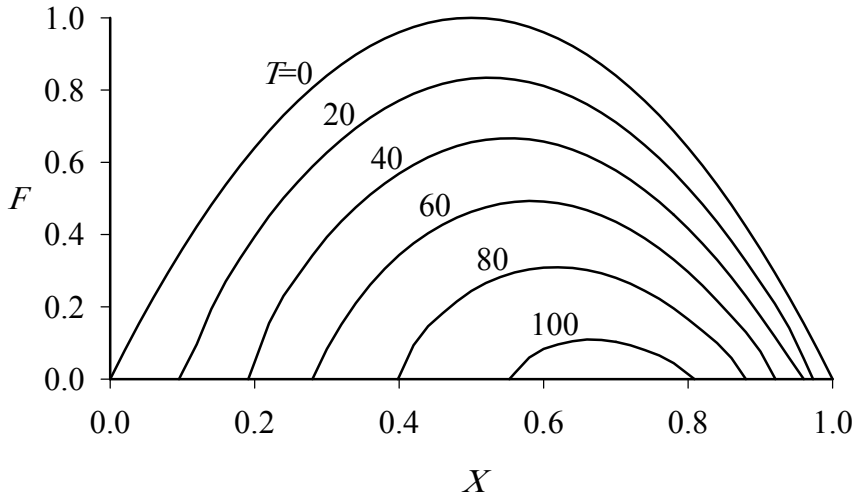

Fig.2. Erosion of hump

The results of the typical case (λ=1,α=0) agree with what one expects. The erosion in the front of the hump is faster than in its back. The originally symmetric hump progressively looses its symmetry. This is obvious in Fig. 2 showing the hump shape at different times of interval 20.

The contamination spreads laterally mainly by diffusion and longitudinally downstream mainly by convection. The contamination boundary, defined to be having concentration of 1%C_s, is shown in its development stage in Fig. 3a and afterwards in Fig. 3b.

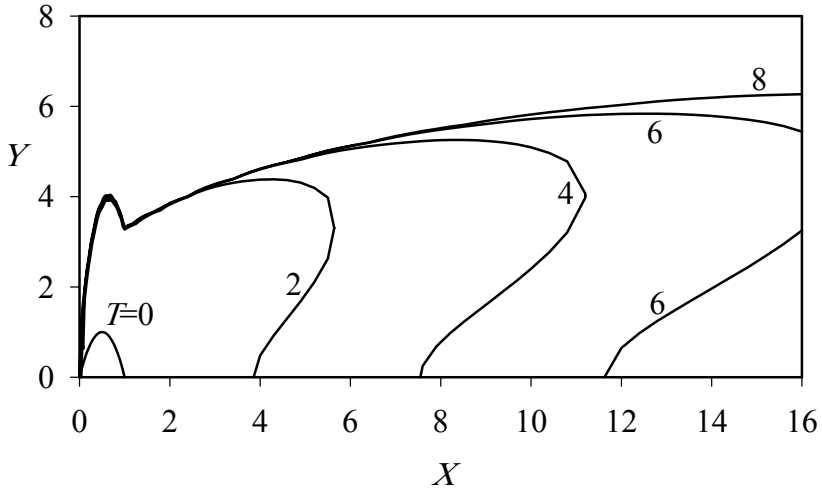

a) early stages ($0 \leq T \leq 8$)

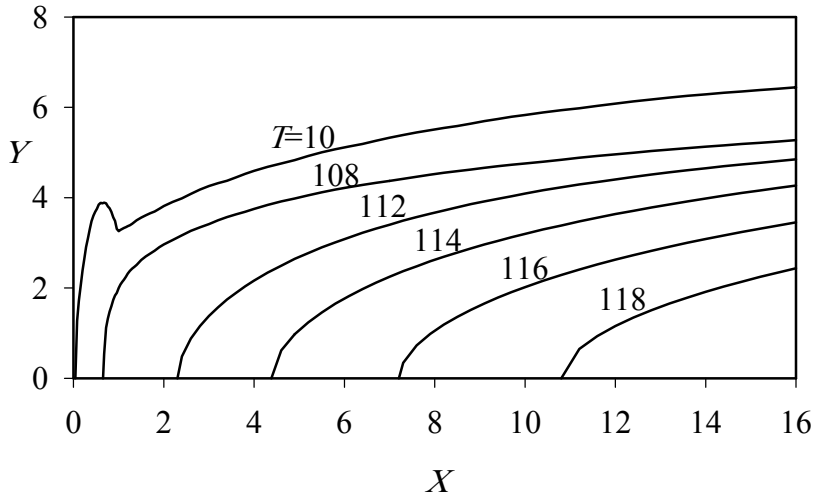

b) later stages ($T \geq 10$)

Fig. 3. Contamination boundary

The contamination boundary expands laterally then approaches a ceiling ($T\approx10$), as the oncoming clean fluid carries the contaminant further and further downstream till it reaches the computational boundary (X=16). With the diminishment of the hump the ceiling falls gradually, and after the hump is completely removed ($T\approx108$) the contamination boundary travels downstream until it departs the computational domain ($T\approx120$).

Figure 4 presents several concentration contours at the instant ($T\approx16$) when the 10%C_s contour reaches its farthest downstream extent. Higher concentration contours, likewise, extend to their farthest but earlier (e.g. at $T\approx9$ for the 20%C_s contour); then retract slowly marking a slight prominence of convection over diffusion.

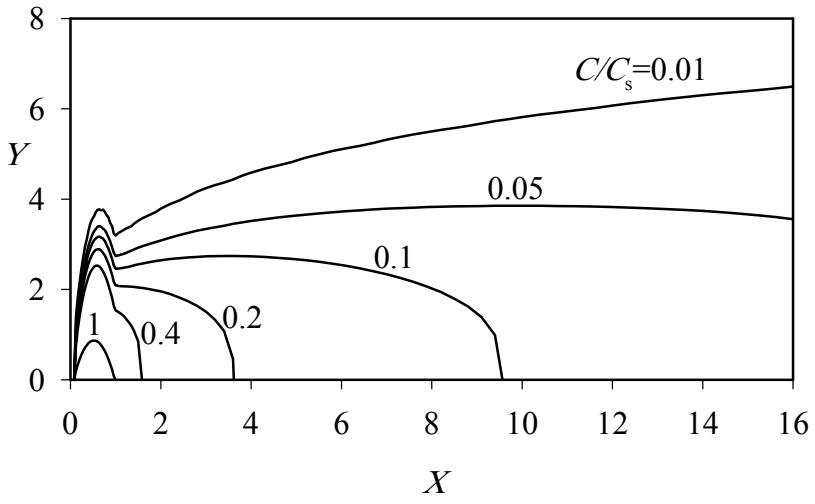

Fig. 4. Concentration contours at T≈16

Decreasing the diffusion parameter λ leads to a decrease in the lateral extent of the contamination as well as in the erosion rate of the hump. This is inferred from Table 1, which presents the calculated values of the contamination ceiling y_c at a typical location (X=10), and the time T_r required for complete removal of the hump, for different values of λ (with α=0). These trends are expected to persist as λ diminishes further, since it has been shown [13] that a "concentration boundary layer" forms close to the surface with the following asymptotic orders. As $\lambda \sim 0$; $X=O(\lambda^0)$, $y=O(\lambda^{1/3})$, $T=O(\lambda^{-2/3})$, $U=O(\lambda^{1/3})$, $v=O(\lambda^{2/3})$, and $C=O(\lambda^0)$. Adherence to these orders is demonstrated in Table 1 by the remarkable agreement among the calculated values and those obtained by modulating the underscored results of λ=1, in accordance with these orders.

Table 1: Effect of λ
on contamination ceiling y_c at X=10, and on removal time T_r

λ	y_c	T_r	y_c	T_r
0.5	4.64	170.1	4.63	171.8
1.0	<u>5.83</u>	<u>108.2</u>	5.83	108.2
2.0	7.33	68.6	7.35	68.2
5.0	9.89	37.6	9.97	37.0
	Calculated		Modulated	

To study the effect of the buoyancy parameter, the values α=-10, 0, 10, and 20 were used (with λ=1). The negative value of α corresponds to the case of a light contaminant diffusing into a heavier fluid [14]. Within this range of α, the results show

minor effect of α on the flow field and the erosion/contamination process. Its main effect is on the pressure; causing it to vary laterally, as expressed by Eq. (1.3). The variation of the surface pressure P_s with α (at T=10) is shown in Fig. 5, in which the case α =0 represents the farfield pressure P_f (as $y\sim\infty$), as well. In the clean part of the flow ($X<X_b$), $P_s=P_f$, as it should. In the contaminated part, positive α is associated with an increase in the specific gravity of the fluid; leading to $P_s>P_f$, while negative α leads to $P_s<P_f$.

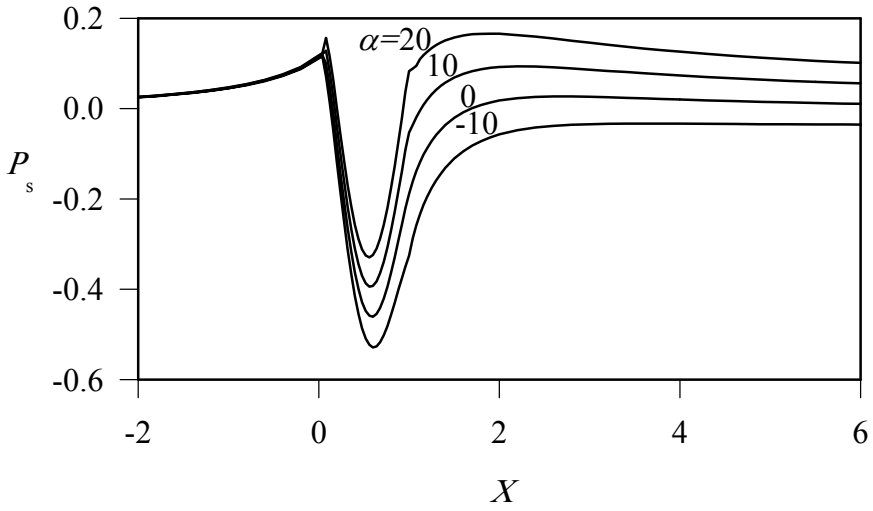

Fig. 5. Effect of α on surface pressure

6. CONCLUSION

The subsonic flow past a horizontal flat surface having an eroding contamination spot- in the form of a hump- has been studied numerically, as a triple deck problem. The difficulties, associated with the erosion of the hump and the contamination of the

flow, have been handled efficiently. The results attest to the validity of the triple-deck model, as well as the numerical method in use. The lateral spread of the contaminant is confined to a neighborhood of the surface that diminishes forming a concentration boundary layer, as the diffusion parameter λ diminishes. Buoyancy causes vertical pressure variations that increase as the buoyancy parameter α increases.

REFERENCES

1. I. J. Sobey, "Introduction to interactive boundary layer theory", Oxford University Press, Oxford, 2000.
2. C. E. Jobe, and O. R. Burggraff, "The numerical solution of the asymptotic equations of trailing edge flow", Proc. Roy. Soc. Lond., **A340 (**1974), pp. 91-111.
3. F. T. Smith, "Laminar flow over a small hump on a flat plate", J. Fluid Mech., **57** (1973), pp. 803-829.
4. M. Napolitano, R. T. Davis, and M. J. Werle, "A numerical technique for the triple-deck problem", AIAA Paper- Number 78-1133, 1978.
5. F. T. Smith, R. I. Sykes, and P. W. M. Brighton, "A two-dimensional boundary layer encountering a three-dimensional hump", J. Fluid Mech., **83** (1977), pp. 163-176.
6. R. I. Sykes, "Stratification effects in boundary layer flow over hills", Proc. Roy. Soc. Lond., **A361** (1978), pp. 225-243.
7. P. W. Duck, "Laminar flow over a small unsteady hump on a flat plate", Mathematika, **25** (1978), pp. 24-35.
8. P. W. Duck, "Laminar flow over unsteady humps: the formation of waves", J. Fluid Mech., **160** (1985), pp. 465-498.
9. R. J. Bodonyi, W. J. C. Welch, P. W. Duck, and M. Tadjfar, "A numerical study of the interaction between unsteady free-stream disturbances and localized variations in surface geometry", J. Fluid Mech., **209** (1989), pp. 285-308.
10. C. W. Jones, and E. J. Watson, "Two-Dimensional Boundary Layers", in: L. Rosenhead (ed.), "Laminar Boundary Layers", Oxford University Press, Oxford, 1966.

11. A. E .P .Veldman, “New, quasi-simultaneous method to calculate interacting boundary layers”, AIAA J., **19** (1981), pp. 79-85.
12. T. M. A. El-Mistikawy, “Separation prevention as an indirect problem based on the triple-deck theory”, AIAA J., **32** (1994), pp.1423-1427.
13. T. M. A. El-Mistikawy, and F. M. N. El-Fayez, “Supersonic triple deck flow past an eroding hump”, Euro. J. Mech./B-Fluids, **24** (2005), pp. 448-456.
14. D. J. Tritton, “Physical Fluid Dynamics”, ELBS and Van Nostrand Reinhold, London, 1979.
15. H. B. Keller, “Numerical methods in boundary-layer theory”, Annual Review of Fluid Mechanics, **10** (1978), pp. 417-433.